

Graphene at High Bias: Cracking, Layer by Layer Sublimation, and Fusing

A. Barreiro,^{*,†,||,⊥} F. Börrnert,^{‡,||} M. H. Rummeli,^{‡,§} B. Büchner,[‡] and L. M. K. Vandersypen[†]

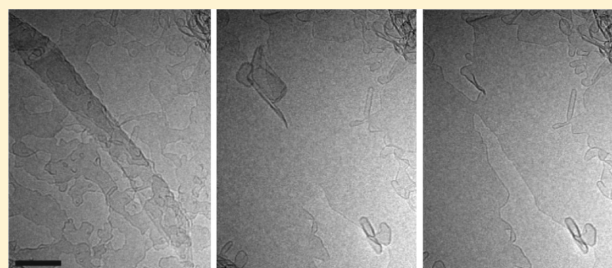
[†]Kavli Institute of Nanoscience, Delft University of Technology, Lorentzweg 1, 2628 CJ Delft, The Netherlands

[‡]IFW Dresden, Postfach 270116, 01171 Dresden, Germany

[§]TU Dresden, 01069 Dresden, Germany

S Supporting Information

ABSTRACT: Graphene and few-layer graphene at high bias expose a wealth of phenomena due to the high temperatures reached. With in situ transmission electron microscopy, we observe directly how the current modifies the structure, and vice versa. In some samples, cracks propagate from the edges of the flakes, leading to the formation of narrow constrictions or to nanometer spaced gaps after breakdown. In other samples, we find layer-by-layer evaporation of few-layer graphene, which could be exploited for the controlled production of single layer graphene from multilayered samples. Surprisingly, we even find that two pieces of graphene that overlap can heal out at high bias



and form one continuous sheet. These findings open up new avenues to structure graphene for specific device applications.

KEYWORDS: Graphene, transmission electron microscopy, nanostructuring, nanosculpting, in situ Joule heating

Since the first isolation of graphene in 2005, this material has attracted intense interest for a wide range of electronics applications.¹ Novel devices such as field-effect transistors (FETs) based on nanoribbons,^{2,3} optoelectronics devices with monolayer-bilayer junctions,^{4,5} and nanometer-spaced electrodes for molecular junctions⁶ require very specific nano-engineering techniques for patterning and structuring the graphene. Conventional lithography is in many cases not sufficient and in situ techniques such as current-induced annealing have proven very useful.⁷ For instance, by applying a high bias, the mobility of graphene can be significantly improved,^{7,8} narrow constrictions that behave as quantum point contacts can be formed,⁹ and nanometer-spaced gaps that are stable at room temperature can be controllably formed.⁶

In this Letter, we perform real-time in situ TEM studies of graphene at high bias. We report a rich variety of phenomena that provide important insights into how to shape graphene or modify its structure (e.g., number of layers) by Joule heating. We observe peeling off of multilayered suspended graphene sheets layer-by-layer locally until only a graphene monolayer remains. Moreover, we are able to controllably narrow down graphene into nanoribbons as narrow as 1 nm, which sustain current densities as high as 6×10^9 A cm⁻², in agreement with a recent report by Lu et al.¹⁰ Surprisingly, we also find that the breakdown current density sharply increases with decreasing width. Finally, two separate but overlapping pieces of graphene can become one continuous sheet again. The results offer a new approach to structuring graphene that is relevant for specific device applications.

Chips with single-layer and few-layer graphene flakes supported by metal contacts were mounted on a custom-built sample holder for TEM with electric terminals, enabling simultaneous TEM imaging and electrical measurements. For imaging, a FEI Titan³ 80–300 transmission electron microscope with a CEOS third-order spherical aberration corrector for the objective lens was used. It operated at an acceleration voltage of 80 kV to reduce knock-on damage. All studies were conducted at room temperature with a pressure of approximately 10^{-7} mbar. Figure 1 shows an image of an electrically contacted few-layer graphene device inside the TEM. The sample fabrication procedure is described in detail in the Supporting Information. In total, we measured 15 devices.

First, we perform in situ current-induced annealing of the suspended graphene devices by taking the samples to the high bias regime, specifically up to 2–3 V.⁷ Temperatures as high as 2000 °C are reached due to Joule heating.^{11,12} As a result, most contaminants from fabrication are removed and we observe in the TEM that we obtain atomically clean graphene devices.

If we increase the bias even further, we reach the high-current limit. In this regime, the samples are at such a high bias that they are close to a complete and irreversible electrical breakdown. Because of this, we increase the bias very carefully in steps of 10 mV until we see that the current flowing through the sample decreases as a function of time, and then keep the

Received: December 1, 2011

Revised: March 12, 2012

Published: March 14, 2012

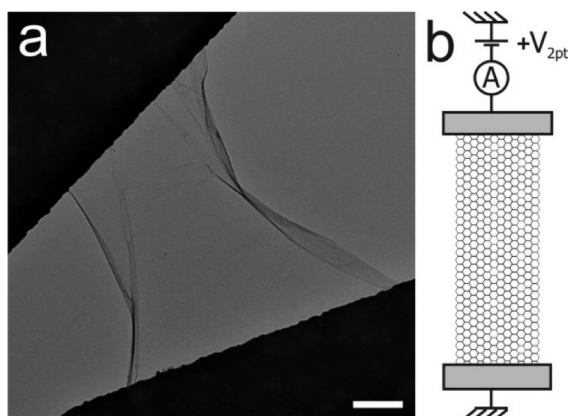


Figure 1. (a) TEM image of an as-fabricated few-layer graphene flake connected to two Cr/Au electrodes. The scale bar is 200 nm. (b) Schematic representation of the measurement setup. The device is voltage biased and the current is measured.

bias constant (typically around 3 V). At this constant bias, we observe that the total current flowing through the sample further decreases over time, which is an indication of carbon atom sublimation.¹¹ The most frequent situation is that a crack forms on one edge of the sample halfway between the electrodes and slowly propagates toward the other edge of the device. This can be understood by the fact that removing an atom from a vacancy edge requires much less energy (~ 7 eV) than that from a perfect lattice site (~ 30 eV).¹³ In few-layer graphene samples, the cracks in the different layers are closely spaced and propagate in the same direction with a similar speed. When the further advanced crack reaches the other side of the sample,¹⁴ it changes direction and moves toward the other crack until the two cuts meet and the sample ends up with two separate but very closely spaced sheets (Figure 2 and Supporting Information video S1).¹¹ A similar mechanism has been reported for the formation of nanometer spaced gaps in mono- and few layer graphene on SiO₂.^{6,15} As explained in detail in section S3 of the Supporting Information, the main driving mechanism of carbon atom sublimation in our experiments should originate from Joule heating.

Importantly, the propagation of cracks can be harnessed to form very narrow graphene nanoconstrictions (GNCs) and can be applied to the formation of nanoribbons. For this purpose, the crack propagation must be controllably stopped before complete breakdown, see Figures 3 and 4, and Supporting Information video S2. In these two specific cases, edges exhibiting a strong contrast can be observed, suggesting a bilayer edge (BLE), which is in contrast to a faint contrast, indicating a monolayer edge (MLE).^{14,16–18} In the measurements corresponding to Figure 4, we observed a stepwise decrease in the current as the constriction was narrowed. From real-time imaging in the TEM, we could infer that these steps corresponded to structural changes in the constriction. Interestingly, the device in Figure 4 originated from merging two separated graphene layers, see Supporting Information Figure S5.¹⁴

Remarkably, these nanometer-sized constrictions are able to hold together the bigger parts of the flake that are connected to the electrodes and exhibit a defect-free lattice as resolved by aberration-corrected high-resolution TEM (AC-HRTEM) in figure 3.

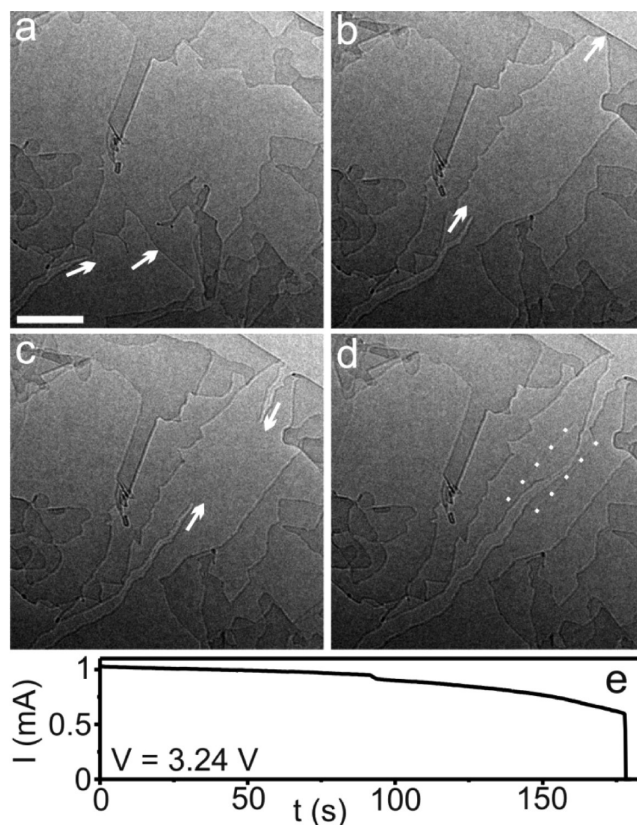


Figure 2. Evolution of a crack. The arrows point in the direction of propagation of the crack. (a) The crack propagates in two different bilayers. The scale bar is 100 nm. (b) The top bilayer crack reaches the edge of the sample and (c) reverses its direction of motion.¹⁴ (d) The two wedges propagate toward each other until they meet. A graphene monolayer region (marked by dotted lines) forms a nanometer spaced gap. The time elapsed between the 4 frames is 100 s (Supporting Information video S1 shows the entire process). (e) The current (I) flowing through the device as a function of time decreases steadily during the electroburning while keeping the bias voltage fixed at 3.24 V. The final breakdown current density is 4.68×10^8 A cm⁻² when normalized to the thickness of a bilayer graphene (0.68 nm).

Moreover, the GNCs are also able to sustain enormous current densities before breakdown (j_{BR}). Indeed, $j_{BR} = 40$ μ A/nm, corresponding to 6×10^9 A cm⁻² if normalized for a graphene thickness of 0.68 nm for the 1 nm wide constriction in Figure 4c, can be extracted from the I – V data in Figure 4e. Recently, a slightly higher j_{BR} has been observed for GNCs sculpted in situ with the TEM beam.¹⁰ For comparison, the j_{BR} of carbon nanotubes (CNTs) corresponds to a current density exceeding 10^9 A cm⁻²,^{19,20} or even up to 4.5×10^9 A cm⁻² for very short (in the 50 nm range) single-wall CNTs,^{21,22} comparable to the j_{BR} that our graphene nanoribbons are able to sustain.

For both CNTs and graphene nanoribbons, j_{BR} is several orders of magnitude larger than in present-day interconnects.²³ It is also around 2 orders of magnitude larger than the values reported for 200 nm wide suspended graphene constrictions,²⁴ and for micrometer-sized few-layer graphene samples.^{11,17} Consistent with those reports, we observe that the breakdown current density j_{BR} sharply decreases with increasing width of the graphene device, down to only 1.2×10^7 A cm⁻² for a 800 nm wide piece (see Figure 5). Indeed, it was not possible to narrow down all the devices to nanoconstrictions. Here the

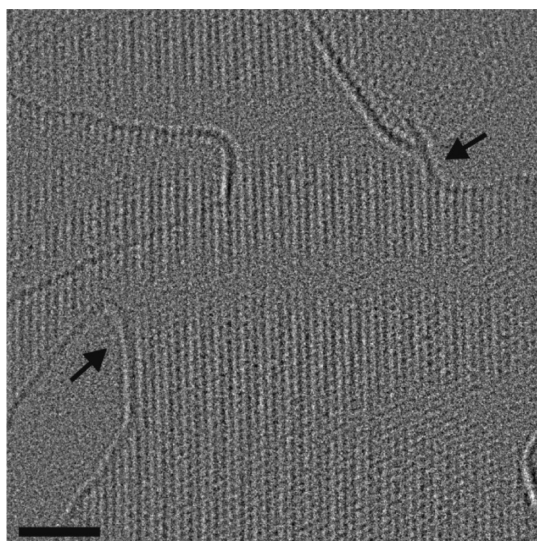


Figure 3. AC-HRTEM micrograph of a narrow bilayer graphene constriction with a very regular and defect-free lattice, formed by controllable electro-burning by crack propagation from the sides. The scale bar is 2 nm. This micrograph has been subjected to a Wiener filter to remove the background and enhance the signal-to-noise ratio.

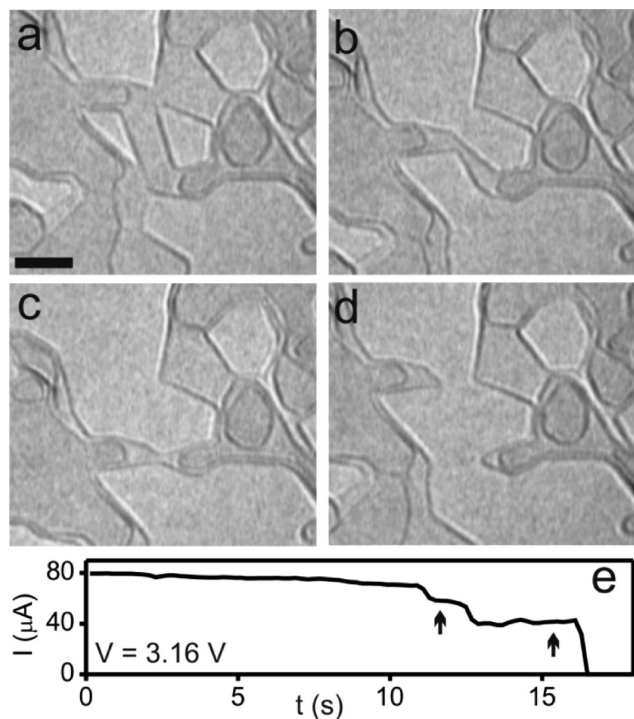


Figure 4. Evolution of a narrow bilayer graphene constriction at high bias. The graphene patches on the bigger parts of the flake grew from amorphous carbon deposited on the sample at zero bias.^{12,25} (a) Two narrow constrictions are connected to two big pieces of graphene. The scale bar is 5 nm. (b) Rupture of one of the junctions, leading to a single narrow constriction with a kink. (c) Removal of the kink and gradual narrowing of the constriction. (d) Rupture of the narrow constriction. The time elapsed between the 4 frames is 18 s. (e) Current (I) as a function of time at a fixed bias voltage $V = 3.16$ V of panels (a–d). The arrows correspond to panel (b) and (c), respectively. The final breakdown current density j_{BR} is 6×10^9 A cm^{-2} when normalized to the thickness of bilayer graphene (0.68 nm).

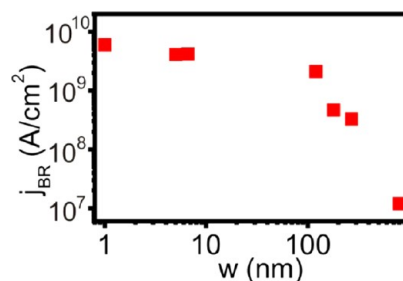


Figure 5. Breakdown current density j_{BR} as a function of width in the range of 1–800 nm.

width of the flake refers to the width of the device just before complete electrical breakdown.

It is surprising that the suspended GNCs are able to sustain a j_{BR} more than 2 orders of magnitude bigger than a micrometer wide suspended graphene. On the basis of the information we have it is difficult to be certain about the origin of this observation. Although we do observe that we have rather clean edges in the GNCs, we do not believe the edges play a role in enhancing j_{BR} as they introduce an additional scattering source as compared to the bulk, which should result in smaller breakdown current densities for narrower ribbons, opposite to what we observe. One possibility why j_{BR} increases for narrower constrictions is a more efficient heat dissipation of the short nanoribbons through the much wider graphene counterparts that connect them to the metal electrodes. Also it could simply be the case that graphene flakes with more adsorbates break down earlier in an uncontrollable manner due to a sudden reaction with the contaminants, leading to a complete electrical breakdown. Cleaner samples allow for a controlled narrowing leading to GNCs, therefore sustaining higher j_{BR} as the breakdown is not triggered by contaminants.

On some occasions, we find that carbon atom sublimation occurs not only in the form of cracks starting from the edges but also in the central area of the flake, eventually leading to layer-by-layer sublimation. For example, during the crack propagation of two BLEs marked by arrows in Figure 6a

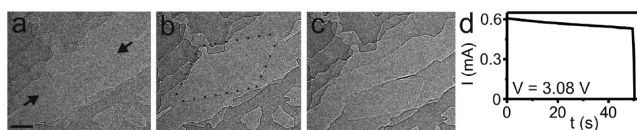


Figure 6. (a) Bilayer graphene sample that was narrowed down by crack propagation from both sides. The arrows point in the direction of crack propagation from both sides. The scale bar is 20 nm. (b) The cracks at the sides stop propagating and a hole forms in the middle of the top layer which expands in a polygonal fashion leaving a monolayer of graphene. The dotted lines are guides to the eye. (c) Electrical breakdown of the device. The time elapsed between the three frames is 50 s. (d) Current as a function of time at $V = 3.08$ V. The breakdown current density j_{BR} is 2.1×10^9 A cm^{-2} .

toward the central region of the flake we found that suddenly one of the two layers developed a hole in the center of the constriction and propagated outward in a polygonal fashion, before the remaining layer(s) eventually broke down (Figure 6 and Supporting Information video S3). The lighter contrast in the broken region and the fact that there were no more lattice fringes at the sides of the flake suggest that a monolayer was present just before breakdown. This finding has been observed not only for bilayer graphene but also for multilayered samples

where layer-by-layer sublimation eventually leads to the formation of single layer graphene (see Figure 7 and Supporting Information video S4).

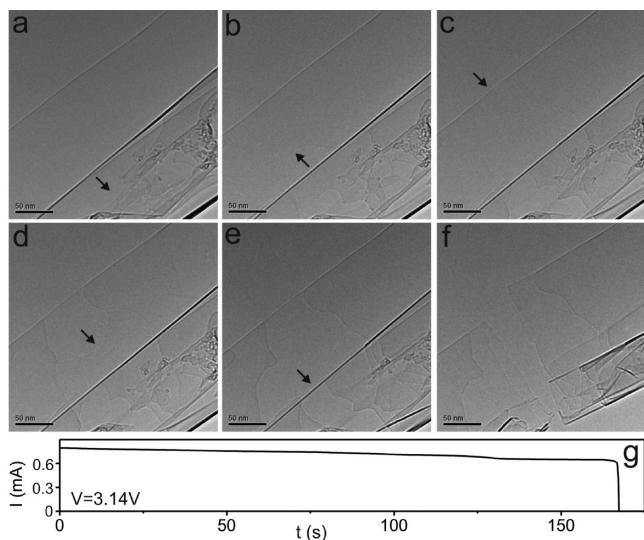


Figure 7. (a–e) Layer-by layer sublimation of a folded few-layer graphene flake until complete electrical breakdown (f). The arrows point in the direction of propagation of the layer sublimation. The time elapsed between the 6 frames is 140 s. (g) Current vs time at $V = 3.14$ V. The breakdown current density j_{BR} is 3.3×10^8 A cm $^{-2}$.

Possible reasons for preferential carbon atom sublimation starting from the center rather than by continuing the crack propagation could be higher temperatures reached in the middle of the flake or the presence of a defect in the lattice from where the atom sublimation ignites. In total, we have observed a similar behavior in three samples while steady crack propagation until the final breakdown was observed in eight devices, illustrating the various types of behavior that occur at high bias, close to electrical breakdown. When sufficiently well understood, controlled sublimation may be used for tailoring layer thickness, for example, by creating damage on purpose in the center and next applying a large bias. On the other hand, sublimation from the center could present a problem for controlled crack propagation and the formation of narrow constrictions if unintentional defects exist in the middle of the flake.

Another interesting event we found when applying a high bias voltage is that two pieces of graphene resulting from the rupture of a flake can overlap and start conducting again, see Supporting Information Figures S5–S8.¹⁴ In Figure 8a,b, the region of overlap can be identified by its darker contrast and by following the dotted lines that are guides to the eye indicating the edges of the respective pieces formed upon rupture. The area of overlap changes over time (Figure 8a,b and Supporting Information videos S5 and S6),¹⁴ and these changes are accompanied by conductance changes of the device, see first arrow in Figure 8g and Supporting Information Figure S6.¹⁴ In Supporting Information Figure S10, several conductance changes can be observed, corresponding to the repeated

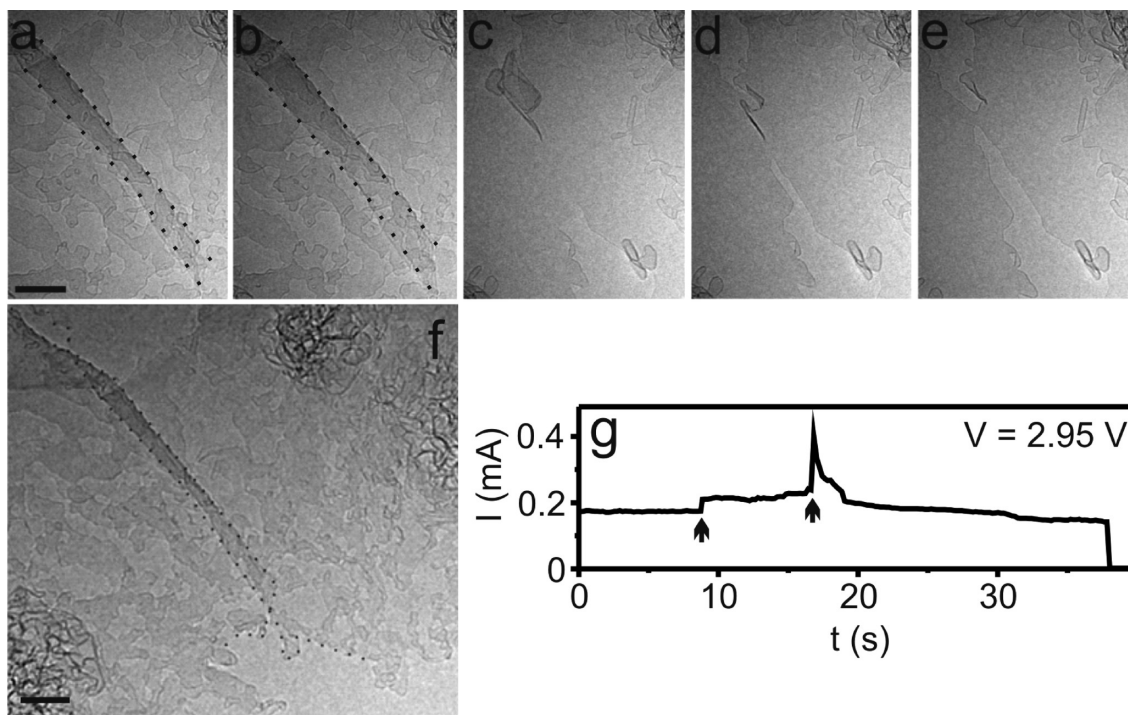


Figure 8. (a,b) TEM images of two overlapping regions of graphene that move as a function of time. The dotted lines are guides to the eye indicating the borders of the two graphene layers. They enclose the region where the two layers overlap (darker contrast in the TEM image) and flake-to-flake electron transport occurs. The scale bar is 20 nm. (c) Sudden healing of the two overlapping flakes and fusing into continuous, seamless bilayer graphene with a smallest width of approximately 60 nm. The constriction next narrows down gradually by atom sublimation from the edges due to Joule heating, reaching a width of (d) 20 and (e) 5 nm, respectively. The time elapsed between the five frames is 35 s (see also Supporting Information video S5). (f) Zoomed out TEM image of panel a. The scale bar is 20 nm. For a further magnified image please see Supporting Information Figure S9.¹⁴ (g) Current as a function of time at $V = 2.95$ V. The arrows correspond to panels (b) and (c), respectively. The breakdown current density j_{BR} is 8.1×10^9 A cm $^{-2}$.

motion of one flake relative to the other, seen in Supporting Information video S6. We have observed overlapping flakes after rupture with changes in conductance on four devices.

Perhaps the most surprising finding is that the overlapping regions can heal to form one continuous, clean graphene layer, see Figure 8c (the graphene patches on top that originated from amorphous carbon have sublimated in the process).^{10,25} The overlap area is very hot as it is located in the central part of the flake and has the highest resistance as there electron transport occurs from flake to flake. As a result of the high temperature, the graphene heals out into a seamless graphene sheet. From the dark contrast of the edges in Figure 8d,e we infer that this is, again, bilayer graphene.

At the moment when the graphene grows together from the two overlapping regions, a sudden increase in conductance is observed, despite the simultaneous reduction in width (second arrow in Figure 8f); this can be expected as the resistance through a seamless graphene sheet is smaller than through two overlapping sheets where the electrons have to hop from one sheet to the other. We note that we have never observed a sudden increase of current upon evaporating graphene; it is the healing that causes the increased conductance. While keeping the bias constant, the newly formed seamless graphene next narrows down gradually by crack propagation from the edges until a constriction of only a few nanometers is formed, see Figure 8d,e.

In conclusion, carbon atom sublimation driven by a high bias can represent a versatile and efficient alternative to beam-driven erosion of carbon atoms for nanostructuring graphene. Via in situ TEM studies in the high current limit, we observe real-time formation of cracks that lead to ultranarrow constrictions, layer-by-layer removal, and the mechanical motion of two disconnected graphene layers one on top of the other that can heal into a perfect defect-free graphene. A more detailed understanding of the dynamics of layer-by-layer peeling and narrowing of few-layer flakes may provide tools for tailoring the graphene layer thickness and lateral dimensions with atomic precision, enabling new device applications. When sufficiently well understood and controlled, this technique could be applied without the visual feedback from in situ TEM measurements, so that it does not rely on expensive equipment.

■ ASSOCIATED CONTENT

■ Supporting Information

Details of the sample fabrication procedure and the experimental methods; effect of the 80 keV TEM electron beam; additional TEM images of the crack formation leading to a narrow constriction and the conductance switches due to the changes in the area of two overlapping graphene flakes; and MWNT formation at the edges of few-layer graphene after electrical breakdown. Movie S1 (SI file 2): Video of the crack propagation in Figure 2, 13 times faster than in real-time. Movie S2 (SI file 3): Video of the formation of the narrow constriction at high bias in Figure 3, four times faster than in real-time. Movie S3 (SI file 4): Video of the sublimation of one of the layers of a bilayer in Figure 6, two times faster than in real-time. Movie S4 (SI file 5): Video of the layer-by-layer sublimation in Figure 7, six times faster than in real-time. Movie S5 (SI file 6): Video of the mechanical switches of two overlapping graphene layers and transformation into a seamless graphene sheet in Figure 8 in real-time. Movie S6 (SI file 7): Video of the two overlapping layers in Figure 8 sliding on top of each other a large number of times, 32 times faster than in

real-time. This material is available free of charge via the Internet at <http://pubs.acs.org>.

■ AUTHOR INFORMATION

Corresponding Author

*E-mail: ab3690@columbia.edu.

Present Address

[†]Department of Physics, Columbia University, New York, New York 10027, U.S.A.

Author Contributions

[‡]These authors contributed equally.

Notes

The authors declare no competing financial interest.

■ ACKNOWLEDGMENTS

We gratefully acknowledge M. Rudneva and H. Zandbergen for help in the early stages of the experiment, G. F. Schneider for help with graphene transfer, and M. Zuiddam for help with the deep reactive ion etching process. Financial support was obtained from the Dutch Foundation for Fundamental Research on Matter (FOM), AGAUR (2010_BP_A_00301), DFG (RU1540/8-1), EU (ECEMP) and the Freistaat Sachsen.

■ REFERENCES

- (1) Novoselov, K. S.; Jiang, D.; Schedin, F.; Booth, T. J.; Khotkevich, V. V.; Morozov, S. V.; Geim, A. K. *Proc. Natl. Acad. Sci. U.S.A.* **2005**, *102*, 10451–10454.
- (2) Han, M. Y.; Oezylmaz, B.; Zhang, Y.; Kim, P. *Phys. Rev. Lett.* **2007**, *98*, 206805.
- (3) Schwierz, F. *Nat. Nanotechnol.* **2010**, *5*, 487–491.
- (4) Avouris, P. *Nano Lett.* **2010**, *10*, 4285–4294.
- (5) Xu, X.; Gabor, N. M.; Alden, J. S.; van der Zande, A. M.; McEuen, P. L. *Nano Lett.* **2010**, *10*, 562–566.
- (6) Prins, F.; Barreiro, A.; Seldenthuis, J. S.; Aliaga-Alcalde, N.; Vandersypen, L. M. K.; van der Zant, H. S. J. *Nano Lett.* **2011**, *11*, 4607–4611.
- (7) Moser, J.; Barreiro, A.; Bachtold, A. *Appl. Phys. Lett.* **2007**, *91*, 163513.
- (8) Bolotin, K. I.; Sikes, K. J.; Jiang, Z.; Fudenberg, G.; Hone, J.; Kim, P.; Stormer, H. L. *Solid State Commun.* **2008**, *146*, 351–355.
- (9) Tombros, N.; Veligura, A.; Junesch, J.; Guimarães, H. D.; Vera-Marun, I. J.; Jonkman, H. T.; van Wees, B. J. *Nat. Phys.* **2011**, *7*, 697–700.
- (10) Lu, Y.; Merchant, C. A.; Drndic, M.; Johnson, A. T. C. *Nano Lett.* **2011**, *11*, 5184–5188.
- (11) Huang, J. Y.; Ding, F.; Yakobson, B. I.; Lu, P.; Qi, L.; Li, J. *Proc. Natl. Acad. Sci. U.S.A.* **2009**, *106*, 10103–10108.
- (12) Westenfelder, B.; Meyer, J. C.; Biskupek, J.; Kurasch, S.; Scholz, F.; Krill, C. E.; Kaiser, U. *Nano Lett.* **2011**, *11*, 5123–5127.
- (13) Warner, J. H.; Rümmeli, M. H.; Ge, L.; Gemming, T.; Montanari, B.; Harrison, N. M.; Büchner, B.; Briggs, G. A. D. *Nat. Nanotechnol.* **2009**, *4*, 500–504.
- (14) Please see Supporting Information.
- (15) Standley, B.; Bao, W.; Zhang, H.; Bruck, J.; Lau, C. N.; Bockrath, M. *Nano Lett.* **2008**, *8*, 3345–3349.
- (16) Liu, Z.; Suenaga, K.; Harris, P. J. F.; Iijima, S. *Phys. Rev. Lett.* **2009**, *102*, 015501.
- (17) Huang, J. Y.; Qi, L.; Li, J. *Nano Res.* **2010**, *3*, 43–50.
- (18) Qi, L.; Huang, J. Y.; Feng, J.; Li, J. *Carbon* **2010**, *48*, 2354–2360.
- (19) Yao, Z.; Kane, C. L.; Dekker, C. *Phys. Rev. Lett.* **2000**, *84*, 2941.
- (20) Bourlon, B.; Glatli, D. C.; Plaçais, B.; Berroir, J. M.; Miko, C.; Forró, L.; Bachtold, A. *Phys. Rev. Lett.* **2004**, *92*, 026804.
- (21) Javey, A.; Guo, J.; Paulsson, M.; Wang, Q.; Mann, D.; Lundstrom, M.; Dai, H. *Phys. Rev. Lett.* **2004**, *92*, 106804.

(22) Park, J.-Y.; Rosenblatt, S.; Yaish, Y.; Sazonova, V.; Ustunel, H.; Braig, S.; Arias, T. A.; Brouwer, P. W.; McEuen, P. L. *Nano Lett.* **2004**, *4*, 517–520.

(23) Hauder, M.; Gstöttner, J.; Hansch, W.; Schmitt-Landsiedel, D. *Appl. Phys. Lett.* **2001**, *78*, 838.

(24) Moser, J.; Bachtold, A. *Appl. Phys. Lett.* **2009**, *95*, 173506.

(25) Barreiro, A.; Börrnert, F.; Avdoshenko, S. M.; Rellinghaus, B.; Cuniberti, G.; Rummeli, M. H.; Vandersypen, L. M. K. arXiv:1201.3131.